A Thesis

On

Synthesis of silica coated potassium ferrite nanoparticles for biomedical applications

Submitted in the partial fulfillment of requirement for the award of

degree of Master of Technology (M. Tech)

In

MATERIALS AND METALLURGICAL ENGINEERING

Submitted by

NOOR HUMAM SULAIMAN

M.Tech (Material Science and Engineering)

Roll No. : 601002007

Supervisor

Dr. N. K.VERMA

Senior Professor

School of Physics and Materials Science

Thapar University, Patiala – 147004

June 2012

Dedicated to my parents and well wishers

Certificate

This is to certify that the report entitled "Synthesis of silica coated potassium ferrite nanoparticles for biomedical applications" submitted by Noor Humam Sulaiman, Roll no. 601002007, in the partial fulfillment of the requirement for the award of the degree of M.Tech (Material Science and Engineering) from the School of Physics & Materials Science, Thapar University, Patiala, is a record of candidate's own work, carried out by her under my supervision and guidance. She has not submitted this material for credit towards any other degree at Thapar University, Patiala or any other university.

Supervisor
Dr. N.K .Verma
Senior Professor
School of Physics & Material Science
Thapar University
Patiala

Countersigned by:

Dr. Kulvir Singh
Head & Professor
School of Physics & Material Science
Thapar University, Patiala

Dr. S. K. Mohapatra
Dean of Academic Affairs
Thapar University, Patiala

Acknowledgment

It gives me profound pleasure to record my heartfelt gratitude to my erudite and revered guide Dr. N. K. Verma, Senior Professor, School of Physics and Materials Science, for his sense of direction, meticulous efforts, for the completion of my work. I am much indebted for his benevolent help, appreciation, encouragement, enlightens and co-operation.

I shall be failing in my duties if I do not express my deep sense of gratitude towards Dr. Kulvir Singh, Professor& Head, School of Physics and Materials Science, who has been a constant source of inspiration, encouragement, supporting for me throughout my studies here.

I would like to specifically thank Dr. O. P. Pandey, Senior Professor, and I would like also to thankful and grateful for Dr. Puneet Sharma Assistant professor and Dr.BhupendraKumar Chudasama Assistant Professor School of Physics and Materials Science, for their generous help, encouragement and good wishes.

I express my cordial thanks to Miss Lavanya Khanna, for her timely help, co-operation, encouragement, and useful discussions. I wish to express my heartfelt thanks to research scholars, Miss Manveen Kaur, Miss Kamal, Miss Geetanjali, Mr. Sanjeev, Mr. Gurmeet Singh and Mr. Jaspal Singh for their ever-available guidance and indispensable comments, which helped me to develop and shape this study in the present form.

I owe my sincere thanks to Mr. Purushotam Kumar Singh for helping me during the course of my work and all the staff members of School of Physics and Materials Science for their support and encouragement.

I would like also to extend my love and thanks to my sisters, my friends who have always been my one of the biggest supporters. Finally, I would like to express my deepest gratitude and love to my parents, without whom I am nothing, for providing me great opportunities, everlasting support, big encouragement and lots of love.

June, 2012
Place: Thapar University, Patiala

(Miss. Noor Humam Suliaman)
(Roll no. 601002007)

Abstract

In the present work, potassium ferrite nanoparticles were synthesized by sol – gel method and the synthesized potassium ferrite nanoparticles were coated with silica by stöber method. The synthesized nanoparticles were characterized by XRD (X-ray diffraction), which revealed the formation of orthorhombic structure of potassium ferrite nanoparticles. The crystallite size using Scherer's formula of potassium ferrite nanoparticles and silica coated potassium ferrite nanoparticles was calculated to be 21 nm and 22.5 nm, respectively. The morphological analysis of the synthesized nanoparticles was done by SEM (Scanning Electron Microscope), TEM (Transmission Electron Microscope), where in case of potassium ferrite nanoparticles, agglomeration was observed; there was reduced agglomeration along with spherical morphology when the potassium ferrite nanoparticles were coated with silica. The EDAX (Energy dispersive X-ray spectroscopy) and FTIR (Fourier Transform Infrared Spectrometer) analysis further confirmed the presence of silica on potassium ferrite nanoparticles. The magnetic analysis using VSM (Vibrating Sample Magnetometer) was also done, in which the magnetic saturation decreased from 23.78 emu/g for potassium ferrite nanoparticles to 3.67 emu/g for silica coated potassium ferrite nanoparticles, attributed to the presence of magnetically dead layer of silica on potassium ferrite nanoparticles.

Contents

List of Figures/Table

Contents

List of Table

Chapter 1 Introduction

Nanotechnology is a broad interdisciplinary area of research, development and industrial activity which has been growing rapidly worldwide for the past decade. It can be defined as the branch of science and engineering where phenomena occur at the nanometer scale (1-100 nm). Generally, nanotechnology deals with design, development, production and application of nanomaterials in devices and systems [1].

Nanoscience is the underpinning science of nanotechnology and it refers to study of phenomena and the manipulation of materials at the atomic, molecular and macromolecular scales, where properties differ significantly from those at a larger scale. Nanoscience is not just the science of small particles but the science in which the materials with small dimension show new physical phenomena, such as high surface to volume ratio, quantum confinement and discretization of energy. Due to these phenomena, the nanomaterials possess different properties giving rise to newer properties as compared to their at bulk counterparts [2].

Nanotechnology encompasses all the sciences, such as physics, chemistry and biology. The synthesis of nanomaterials is done by chemical methods, in which the shape and size of the synthesized nanomaterials can be controlled by optimizing various parameters of the reaction procedure as concentration of precursors, temperature variation, pH of reaction, addition of catalyst, etc. The synthesized nanomaterials can be further applied in physics and biology. This gives rise to newer and better technologies which have the potential and capability to modernize every appearance of science and technology. In fact, one can say that nanotechnology has managed to penetrate every field and is completely capable of transforming all the arenas of science and technology. A lot of attraction in nanotechnology stems from the fact that technique from a single discipline can be used in other disciplines, yielding many novel and potential applications as well as challenges. The advent of nanotechnology started from famous talk by Richard Feynman entitled "There's Plenty of Room at the Bottom," [3]. Feynman highlighted the importance of controlling and manipulating on a small scale. However, Norio Taniguchi (1912-1999) used for the first time the term “nanotechnology” in 1974 in a technology production paper that created objects and features of nanometer order [4, 5].

On reducing of particle size, surface to volume ratio increases, discretization of energy bands occur, quantum confinement effects come into play. This size dependent effect brings about a major change in the mechanical, electrical, optical or magnetic properties of the material, enabling the nanomaterials to behave differently from its bulk counterpart. This change can be further used for developing newer and improved technologies, thereby making nanotechnology a potential tool for renewing every feature of electronics, optics, photonics or mainstream biomedical field.

Magnetic nanoparticles have attracted great interest owing to their magnetic properties and biocompatibility, and many researchers have attempted to prepare magnetic nanoparticles with high functionality. The surface modification of magnetic nanoparticles by organic, inorganic molecules is also important for biological applications as targeted drug delivery, Magnetic Resonance Imaging (MRI), Bio-sensing, Molecular imaging, Gene delivery, Medical diagnosis, Therapy giving rising to the field called Biomedical Nanomagnetics. This field is widely scrutinized and attracting researchers towards it, because of the promising results which can revolutionize the area of biomedicine and bring forth better, improved, economical diagnostics and therapy treatments, with an additional advantage of reduced side effects. A safe and targeted drug delivery could improve the performance of some classic medicines already on the market, and moreover, will have implications for the development and success of new therapeutic strategies such as anticancer drug delivery, peptide and protein delivery and gene therapy.

Magnetic nanoparticles (MNPs) have been developed as an important strategy to deliver conventional drugs, recombinant proteins, vaccines and more recently, nucleotides. Magnetic nanoparticle carriers consist of three functional parts:-

1. Magnetic core
2. Surface coating
3. Biomolecular entity (anti-cancer drug)

Several biomedical applications require core-shell magnetic NPs. They are composed of a metal or metallic oxide core, encapsulated in an inorganic or a polymeric coating that renders the particles biocompatible, stable, and may serve as a support for biomolecules [6].

Their magnetic properties enable these particles to be used in numerous applications, belonging to one or more of the following groups:

1. Magnetic contrast agents in magnetic resonance imaging (MRI) [7].
2. Hyperthermia agents, where the magnetic particles are heated selectively by application of a high frequency magnetic field. In thermal ablation / hyperthermia of tumors [7].
3. Magnetic vectors that can be directed by means of a magnetic field gradient towards a certain location, such as in the case of the targeted drug delivery. The scientific properties of magnetic NPs to obtain medical breakthroughs in diagnosis, and drug delivery [7].

The other important point is the coating or the surface functionalization of the magnetic nanoparticles. The biomedical applications need special surface coating of the magnetic nanoparticles, which should not only be non-toxic and biocompatible but also allow a targetable delivery with particle localization in a specific area. To this effect, most work in this held has been done in improving the biocompatibility of the materials, but only a few scientific investigations and developments have been carried out in improving the quality of magnetic particles, their size distribution, their shape and surface in addition to characterizing them to get a protocol for the quality control of these particles. Nature of surface coatings and their subsequent geometric arrangement on the nanoparticles determine not only the overall size of the colloid but also play a significant role in the bio distribution of nanoparticles in the body.

The types of specific coating or derivatization, for these nanoparticles depend on the end application and should be chosen by keeping a particular application in mind, whether it is aimed at inflammation response or anti-cancer agents. Magnetic nanoparticles can bind to drugs, proteins, enzymes, antibodies, or nucleotides and can be directed to an organ, tissue, or tumor using an external magnetic field or can be heated in alternating magnetic fields for use in hyperthermia.

Iron oxide magnetic nanoparticles (MNPs) alone are suitable for a broad spectrum of applications, but the low stability and heterogeneous size distribution in aqueous medium represent major setbacks [8]. These setbacks can however be reduced or diminished through the coating of MNPs with various polymers, especially biopolymers such as polysaccharides. Polysaccharides are biocompatible, non-toxic and renewable; in addition, they possess chemical groups that permit further functionalization of the MNPs. Multifunctional entities can be created through decoration with specific molecules e.g. proteins, peptides, drugs, antibodies, biomimetic ligands, transfection agents, cells, and other ligands. MNPs and several polysaccharides (Agarose, Alginate, Carrageenan, Chitosan, Dextran, Heparin, Gum Arabic, Pullulan and Starch), inorganic coatings of silica, gold can be functionalized on the surface of MNPs.

The coatings on the magnetic nanoparticles serve many purposes. Stabilizers such as polymers, surfactants, inorganic coatings covering the surface of the nanoparticles are required as it:

1. Provide steric or ionic stabilization of magnetic particles against aggregation [9]
2. Increase their biocompatibility
3. Prevent leaching of potentially toxic component into the body during in vivo applications
4. Protect against corrosion [10]
5. Evade Reticuloendothelial System (RES) system [11], Help in binding various biological ligands to the nanoparticle surface [12].

Much research has been carried out on synthesis and characterization of iron oxide [13], cobalt ferrite [14], nickel ferrite [15], manganese ferrite [16], magnesium ferrite [17], and zinc ferrite nanoparticles [18]. The metal based ferrite nanoparticles have been synthesized by various methods as sol-gel auto combustion, evaporation condensation, template-based electrochemical synthesis, spray pyrolysis, micro-emulsion technique, reverse micelle, hydrothermal, co-precipitation [15]. The magnetic properties of these nanoparticles used in medical, electronic and recording industries depends significantly on their size, shape,

purity and magnetic stability [15]. There is a widespread research on iron oxides and metal based ferrite, including both fundamental research and applications, such as mineralogy, biology, chemistry and medicine [19].

The literature was reviewed in detail, in order to gain and gather optimum information as to the genesis and the applications of the work.

Kim et al. [20] have presented a very detailed review on the multifunctional nanostructured materials with possible applications in multimodal imaging, simultaneous imaging and therapy. They have regarded them as novel bioimaging, diagnostic, and therapeutic agents for the future medical field. The review also has given an insight into the different groups and their research work, carried out in this field wherein superparamagnetic iron oxide nanoparticles have been coated with silica and further applied for biomedical purposes. Along with all the information regarding the research work, they have also raised important attention towards the biocompatibility of the multifunctional nanomaterials. In order for them to be used in clinics in the future, many issues including the biocompatibility, toxicity, in vivo targeting efficacy, and long term stability of the multifunctional nanoparticles need to be addressed. Especially, toxicological studies of the nanoparticles are necessary before they can be used in humans. The undesirable effects of the nanoparticles should be removed prior to their use.

Sahoo et al. [21] and Ochekpe et al. [22] have discussed in detail the different nanomaterials employed for targeted drug delivery. Polymeric nanoparticles, Ceramic nanoparticles, Polymeric micelles Dendrimers, Liposomes, Nanocrystals *(regarding quantum dot attachment with the nanoparticle, biological entity and their further applications for florescence studies in biology)*, Magnetic nanoparticles for drug delivery and imaging, have been extensively employed for biomedicine applications with a comprehensive detail about the merits and demerits of the all the above mentioned vehicles. The drug of interest is dissolved, entrapped, adsorbed, attached or encapsulated into the nanoparticle matrix. Depending on the method of preparation, nanoparticles, nanospheres or nanocapsules can be obtained with different properties and release characteristics for the encapsulated therapeutic agent. Nanoparticles were effective in sustaining intracellular dexamethasone levels, thus allowing a more efficient interaction with the glucocorticoid receptors which are cytoplasmic. Micro- and nanoparticles are capable of enhancing immunization. Targeted delivery can be achieved by either active or passive targeting. Active targeting of a therapeutic agent is achieved by conjugating the therapeutic agent or the carrier system to a tissue or cell-specific

ligand. Passive targeting is achieved by coupling the therapeutic agent to a macromolecule that passively reaches the target organ. Ceramic nanoparticles have several advantages such as the preparative processes are relatively similar to the well-known sol-gel process, require ambient temperature condition, and can be easily prepared with the desired size, shape and porosity. Their ultra-low size (less than 50 nm) can help them evade by the reticulo-endothelial system (RES) of the body.

Liong et al. [23] synthesized superparamagnetic iron oxide nanocrystals, which were encapsulated inside mesostructured silica spheres that were labeled with fluorescent dye molecules and coated with hydrophilic groups to prevent aggregation.

Li et al. [24] synthesized Doxorubicin (DOX) conjugated magnetic silica nanoparticles (DOX–Fe_3O_4–SiO_2), fabricated using a new one-pot method. The DOX–Fe_3O_4–SiO_2 nanoparticles showed a significantly lower drug release rate than the control silica nanoparticles due to the urea linkage (–NHCONH–) between the DOX and the inorganic nanoparticles. Therefore, the DOX–Fe_3O_4–SiO_2 nanoparticles have a great application potential in the treatment of cancer using magnetic targeting drug-delivery technology.

Wu et al. [25] synthesized porous nanorods with compositions including both β-FeOOH and α-Fe_2O_3. The derived porous nanorods were engineered to assemble with four layers of polyelectrolytes (polyacrylic acid (PAA)/ polyethylenimine (PEI)/PAA/PEI) on their surfaces as polyelectrolyte multilayer nanocapsules. Fluorescein isothiocyanate (FITC) molecules were loaded into the polyelectrolyte multilayer nanocapsules in order to investigate drug release and intracellular delivery in Hela cells. Cytotoxicity measurements demonstrate that the native nanorods and the polymer coated nanorods have excellent biocompatibility in all dosages between 0.1 $ngmL^{-1}$ and 100 $mgmL^{-1}$.

Kommaredi et al. [26] synthesized superparamagnetic microspheres by incorporating nanometre sized iron oxide crystals into micron-sized phenolic poly (p-ethylphenol) polymer particles. SQUID (Superconducting quantum Interface device) generated magnetic hysteresis loops exhibiting zero remanence and coercivity for the ferrite-polymer composite, indicating superparamagnetic nature of the composite.

Burke et al. [27] synthesized iron oxide - polymer nanocomposite by thermal decomposition of iron pentacarbonyl in the presence of ammonia and polymeric dispersants.

Polyisobutylene and polyethylene based dispersants yielded more uniform particle sizes. Smaller sized nanoparticle composite proved to be superparamagnetic but with low magnetic saturation as compared to larger particle composite in which hysteresis was observed along with higher magnetization.

Chen et al. [28] used a modified aqueous sol-gel route using ultrasonic power for the silica coating of indium tin oxide (ITO) nanoparticles. In this approach, organosilane with an amino functional group was first used to cover the surface of as-received nanoparticles. This process resulted in a thin but homogeneous coverage of silica on the particle surface. Particles coated with a layer of silica show better dispersability in aqueous and organic media compared with the untreated powder.

Chen et al. [29] synthesized three types of iron oxide magnetic nanotubes, i.e., hematite, maghemite, and magnetite, using template and hydrothermal methods, and the effects of synthesis methods on the morphological and crystalline properties of the synthesized magnetic nanotubes were analyzed. The magnetization properties of the three types of synthesized magnetic nanotubes and their responses to external magnetic fields were studied. To explore their applications in drug delivery, the drug loading and release capabilities of the synthesized magnetic nanotubes were investigated.

The nanocrystalline cobalt ferrites have been synthesized using reverse micelle method [30, 31], co-precipitation method [32-34] and sol-gel auto combustion method [35, 36]. K. E. Scarberry [30] investigated the biomedical applications of cobalt spinel ferrite nanoparticles for cancer cell extraction and drug delivery.

Manganese ferrite nanoparticles have also been studied for biomedical applications. They have been employed as contrast agents in Magnetic Resonance Imaging (MRI) and can be considered as a potential magnetic carrier for drug delivery, but not much work has been done on the latter. Esteves et al. [37] synthesized superparamagnetic Mn/Zn ferrite nanoparticles of median diameter 15-17 nm by salt coprecipitation method and coated them with biologically compatible sugar carboxymethyl dextran (CDMx) by physical adsorption and studied their cytotoxicity tests, indicating its viability of above 80% for a conc. of 7.5mg/ml. Yang et al. [38] also synthesized $MnFe_2O_4$ nanoparticles and investigated the MRI contrast agent capabilities of $MnFe_2O_4$. The synthesized $MnFe_2O_4$ were non toxic for concentration of 200µg/ml.

Yin et al. [39] investigated the effects of particle size and surface coating on the cytotoxicity of nickel ferrites. The surfactant used in this case was oleic acid and they found that for the uncoated nickel ferrites, cytotoxicity was independent of particle size within the given mass concentration and surface area accessible to the cells but for nickel ferrites coated with oleic acid, the cytotoxicity significantly increased when one or two layers of oleic acid were deposited. Larger sized particles (150$\pm$ 50 nm) showed a higher toxicity than smaller particles (10 $\pm$ 3 nm).

Voit et al. [40] have presented the study on the magnetic behavior of nanosized iron oxide particles with different surfactants (sodium oleate, PVA and starch) in a ferrofluid. The effect of the coating material, and different particle concentrations in the ferrofluid have been magnetically investigated to determine the effective magnetic particle size and possible interaction.

J. Xu and H. Yang [41] successfully synthesized Magnetite (Fe_3O_4) nanoparticles by sol–gel method. The results indicated that the size, the corresponding saturation magnetization value and coercivity value of Fe_3O_4 nanoparticles increase with the increase of synthesized temperature.

Amtenbrink et al. [42] explained the synthesis and coating of nanoparticles for *in-vivo* and *in-vitro* studies. The potential toxicity of such material is not only related to their nanosize nature but especially to their surface properties, which is the determining factor for cellular uptake and cytotoxicity, whereas the type of particle does not seem to play such an important role.

N. Tran and T. J. Webster. [43] have discussed magnetic nanoparticles used in drug delivery and hyperthermia treatment for cancer and for more effective therapeutic treatments, the materials with highly saturated magnetization (such as transition metals (Fe, Co, Ni) or metal oxides (Fe_3O_4, γ-Fe_2O_3) are usually considered. Although pure metals possess the highest saturation magnetization, they are highly toxic and extremely sensitive to oxidation; therefore, without a further appropriate surface treatment such pure metal nanoparticles are not relevant for biomedical applications. In contrast, ferrites are less sensitive to oxidation and therefore, can give a stable magnetic response. Recent studies have demonstrated that magnetite (Fe_3O_4) and maghemite (γ-Fe_2O_3) are very promising candidates due to their biocompatibility and relative ease to functionalize (for example with polymers such as

dextran, polyethylene glycol (PEG), polyvinyl alcohol (PVA) or functional groups such as thiols, amines and carboxyls) for a wide range of applications.

K. Maaz and S. Karim [15] synthesized nickel ferrite ($NiFe_2O_4$) nanoparticles by co-precipitation route using stable ferric and nickel salts with sodium hydroxide as the precipitating agent and oleic acid as the surfactant, yielding single-phase nickel ferrite nanoparticles in the range 8–28nm depending up on the annealing temperature of the samples during the synthesis. Magnetic saturation, coercivity, remanence changed drastically as the particle size reduced to the nanometric range.

Andrade et al. [44] prepared silica coated magnetite nanoparticles with different types of alcohols, and various volume ratios of ethanol to water ($V_{E/W}$). The feeding amount of catalyst and TEOS (Tetraethoxysilane) were also varied and the synthesis products were carefully characterized.

Tomitaka et al. [45] studied the biocompatibility of Fe_3O_4 (20-30 nm), $ZnFe_2O_4$ (15-30 nm) and $NiFe_2O_4$ (20-30 nm) using a cytotoxicity cell viability assay. The Fe_3O_4 particles were found to be biocompatible on Hela cells. The survival rate of Hela cells exposed to Fe_3O_4, $ZnFe_2O_4$ and $NiFe_2O_4$ at the concentration of 10µg/ml for 24 or 48h was above 80%. At the concentration of 100µg/ml, however, the cells exposed to $ZnFe_2O_4$ and $NiFe_2O_4$ showed low viability of 77.6% and 70.5% for 24h, and 59.4% and 52.4% for 48h, respectively. So, at higher concentrations, $ZnFe_2O_4$ and $NiFe_2O_4$ showed lower cell viability and at concentration lower than 10µg/ml, the three ferrites were non-toxic.

However, use of these metal ferrite nanoparticles in biomedical research can be hampered by high toxicity of the transition metals (Ni, Mn and Co). Non permeable coatings are needed to prevent leaching of these metals. So, the need of the hour is to synthesize highly bio favourable ferrites which exhibit superparamagnetic behaviour with no toxicity threat so that even if leaching does occur the metal used should not cause any harm to the body but can be metabolised by the body and for the same, potassium metal can be considered as good candidate.

3.1 Gaps in Research

From the review of literature, it has been found that the following areas are not much explored till now. Following is the gap in the present study:

- Functionalization of potassium ferrite nanoparticles with silica.

3.2 Objectives

1. Synthesis of potassium ferrite nanoparticles by sol – gel method.
2. Functionalization of synthesized potassium ferrite nanoparticles with silica.
3. Characterization of synthesized potassium ferrite nanoparticles and silica coated potassium ferrite nanoparticles; structurally by X-ray diffraction (XRD), morphologically by Scanning Electron Microscopy (SEM), Transmission Electron Microscopy (TEM).
4. Confirmation of functionalized nanoparticles by Fourier Transform Infrared Spectrometer (FTIR).
5. Magnetic characterization of nanoparticles by Vibrating Sample Magnetometer (VSM).

3.3 Methodology

Following steps will be taken to achieve the objectives:

- **Synthesis of potassium ferrite nanoparticles:** The synthesis will be done by sol-gel method, using ethylene glycol as the solvent and citric acid as the chelating agent.
- **Structural Analysis:** XRD characterization will be done to know about the crystal structure and crystallinity.
- **Morphological Characterization:** The morphology of the synthesized product will be examined by SEM, EDAX and TEM.
- **Functionalization of potassium ferrite nanoparticles:** The synthesized potassium ferrite nanoparticles will be functionalized with silica by Stöber Process.

- **Fourier Transform Infrared Spectrometer (FTIR):** The silica functionalization will be confirmed by FTIR.
- **Magnetic measurement:** The VSM characterization will be performed to study the magnetic behavior of synthesized materials, along with all the characterizations mentioned above.

4.1 Synthesis of nanomaterials

For the syntheses of nanomaterials and nanostructures, two approaches are mainly used, they are, top-down and bottom-up.

4.1.1 Top –down approach

It implicates the breaking down of the bulk material into nano sized structures or particles. 'Top down' is realized by breaking, cutting or etching techniques, which is achieved by bulk or film machining, surface machining and mold machining occupying lithography. Bulk machining makes use of photolithography, which applies the etching process while mold machining uses soft lithography [46, 47].

Top –down approach involves:

1. High energy milling
2. Chemical mechanical milling
3. Vapour phase condensation
4. Electro-explosion
5. Laser ablation
6. Sputtering

4.1.2 Bottom- up approach

It is about the buildup of a material from the bottom, atom-by-atom, molecule-by-molecule, or cluster-by-cluster. The bottom up approach of nanomaterials synthesis first forms the nanostructured building blocks (nanoparticles) and then collects these into the final material, as shown in fig.1 [46].

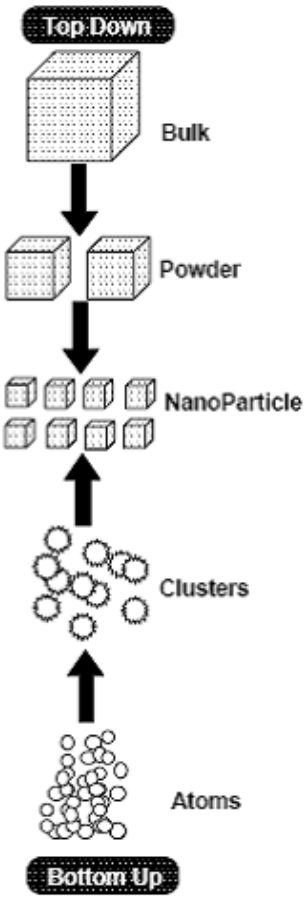

Figure 1 Schematic variety of nanostructure synthesis and assembly approaches

The buildings blocks may be manipulated through controlled chemical reactions to self assemble and make nanostructures such as nanotubes and quantum dots [46, 47].

Bottom–up approach involves:

1. Solution combustion method
2. Sol –gel method
3. Microemulsion
4. Reverse micelle synthesis
5. Chemical precipitation synthesis

In the present work, we will be synthesizing nanoparticles with the sol-gel method, so it has been studied in detail as below.

4.2 Sol-gel method

The sol-gel process is a wet chemical technique widely used in the field of material science and ceramic engineering. Such methods are used primarily for the fabrication of materials (typically a metal oxide) [48]. The sol-gel process, as the name implies, involves the evolution of inorganic networks through the formation of a colloidal suspension (sol) and gelation of the sol to form a network in a continuous liquid phase (gel). The starting material is processed to form a dispersible oxide and forms a sol in contact with water or dilute acid [48]. During the process, the sol yields the gel, and the sol/gel transition controls the particle size and shape. Sol-gel processing refers to the hydrolysis and condensation of alkoxide-based precursors [48]. The reactions involved in the sol-gel chemistry is based on the hydrolysis and condensation of metal alkoxides M (OR), it can be described as follows:

$$MOR + H_2O \rightarrow MOH + ROH \text{ (hydrolysis)}$$

$$MOH + ROM \rightarrow M\text{-}O\text{-}M + ROH \text{ (condensation)}$$

The sol-gel process can be characterized by a series of distinct steps:

I. The first step consists of the formation of different stable solutions of the alkoxide or solvated metal precursor (the sol).

II. In the second step, gelation begins, which results in the formation of an oxide - or alcohol - bridged network (the gel) by a polycondensation or polyesterification reaction that results in a dramatic increase in the viscosity of the solution.

III. The third step is the aging of the gel (also called Syneresis), during which the polycondensation reactions continue until the gel transforms into a solid mass, accompanied by contraction of the gel network and expulsion of solvent from gel pores. It is referred to as coarsening, phenomenon by which smaller particles are consumed by larger particles during the growth process and phase transformations may occur concurrently with syneresis.

IV. The fourth step is drying of the gel, when water and other volatile liquids are removed from the gel network. This process is complicated due to fundamental changes in the structure of the gel. The drying process has itself been broken into four distinct steps: (i) the constant rate period, (ii) the critical point, (iii) the falling rate period, (iv) the second falling rate period. If isolated by thermal evaporation, the resulting monolith is termed a xerogel. If the solvent (such as water) is extracted under supercritical or near super critical conditions, the product is an aerogel.

V. The fifth step involves dehydration, during which surface - bound M-OH groups are removed, thereby stabilizing the gel against rehydration.

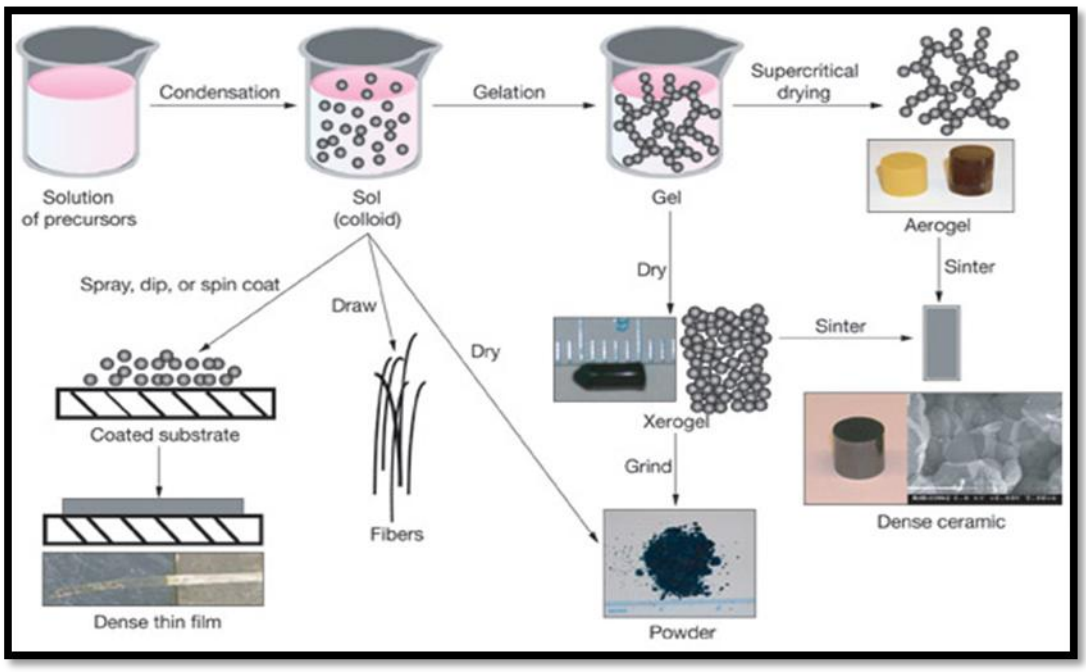

Figure 2 Schematic representation of sol-gel process for synthesis of nanomaterials

The major technical difficulties to overcome in developing a successful bottom-up approach is controlling the growth of the particles and then stopping the newly formed particles from agglomeration as shown in fig. 2 [49].

4.3 Stöber Processes

Silicon is present in environment in different forms. Although it is not found in nascent form but it is always present in combination with oxygen (silica) or hydroxides (silicic acid) [50]. 78% of earth's crust consists of silicon and oxygen compounds, both amorphous and crystalline compounds for example quartz, flint, opal, silicates etc. Silicon is also present in dissolved form in the oceans as silicic acid. Also silica is found in living organisms like sponges, grasses, algae (for example, diatoms) [50].

The Stöber process is a physical chemistry process for the generation of monodispersed particles of silica. The process was discovered in 1968 by Werner Stöber. The Stöber process used for the preparation of spherical and monodispersed silica nanoparticles colloids by means of hydrolysis of silicone alkoxides such as tetraethyl

orthosilicate (TEOS) and subsequent condensation of silicic acid in alcoholic solutions (ethanol) in the presence of water and a base catalyst (ammonia aqueous solution). The particle size distribution also becomes broader when longer-chain alcohols are used as solvents [50]. Like any other synthesis of colloids, the diameters of silica particles from the Stöber process are mainly controlled by the relative contribution from nucleation and growth. The hydrolysis and condensation reactions provide precursor species and the necessary supersaturation for the formation of particles [50, 51]. During the hydrolysis reaction, the ethoxy group of TEOS reacts with the water molecule to form intermediate [Si $(OC_2H_5)_{4-X}$ $(OH)_X$] with hydroxyl group substituting ethoxy groups. Moreover, ammonia works as a basic catalyst to this reaction; the hydrolysis reaction is probably initiated by the attacks of hydroxyl anions on TEOS molecule and it observed the hydrolysis reaction, the condensation reaction occurs immediately [50, 51]. The hydroxyl group of intermediate [Si $(OC_2H_5)_{4-X}$ $(OH)_X$] reacts with either the ethoxy group of other TEOS (alcohol condensation) or the hydroxyl group of another hydrolysis intermediate (water condensation) to form Si-O-Si bridges. Furthermore, it was also claimed that the rate of water condensation is thousands times faster than the alcohol condensation [50, 52].

4.4 Synthesis of potassium ferrite nanoparticles by sol-gel process

The synthesis of potassium ferrite nanoparticles was done by sol-gel method. This process consists of evolution of inorganic network formation of a colloidal suspension (sol) and gelation of the sol to form a network in a continuous liquid phase (gel). Following is the step-wise procedure for the synthesis of potassium ferrite nanoparticles:-

- Stoichoimetric ratio of Potassium Nitrate (KNO_3), Ferric Nitrate ($Fe(NO_3)_3$) and Citric Acid ($C_6H_8O_7.H_2O$) were taken, dissolved in distilled water. The solutions were mixed on a magnetic stirrer at 80°C.
- After sometime a fixed amount of ethylene glycol was added to the above mixture drop wise with continuous stirring and heating.
- During the reaction, it was noticed that the solution became viscous (converting to gel). On further heating, brown colored powder was obtained. The powder was cooled for some time and then was washed with ethanol six times.
- After washing, the powder obtained was dried in oven for 12 hour.

- The obtained powder was calcined at 500 °C for 3 hour; finally potassium ferrite nanoparticles were obtained.

4.5 Synthesis of silica coated Potassium ferrite nanoparticles

After the above synthesis, silica coating on the potassium ferrite nanoparticles was performed by Stö ber process. Following is the step-wise procedure used:-

- ✓ Stoichoimetric ratio of potassium ferrite nanoparticles, ammonia solution, Tetraorthosilicate ($C_8H_2O_4Si$) was taken. In a beaker, potassium ferrite nanoparticles, ammonia solution and ethanol, distilled water were added and ultrasonicated for 20 minute.
- ✓ In the next step, the above solution was mechanically stirred and Tetraorthosilicate ($C_8H_2O_4Si$) was added dropwise and was stirred for 12 hour.
- ✓ After 12 hour stirring, the nanoparticles were magnetically separated.
- ✓ The solution was washed with ethanol by centrifugation. The process was repeated five times.
- ✓ The particles were dried in the oven at 60 °C for 12 hour. Finally, silica coated potassium ferrite nanoparticles were obtained.

4.6 Characterization Techniques

Success in devising and collecting systems on the scale of nanometers require a deeper understanding of the basic processes and phenomena involved. Hence, one of the current key objectives is to adapt and develop a range of techniques that can characterize the structural, thermal, electronic, magnetic, dielectric, composition, electrical and optical properties of the nanostructured systems [53]. These techniques include X-Ray Diffraction (XRD), Transmission Electron Microscope (TEM), Scanning Electron Microscope (SEM), Energy Dispersive X-Ray Spectroscope (EDAX), Vibrational Sample Magnetometer (VSM), Fourier Transform Infrared Spectroscope (FT-IR).

4.6.1 X-Ray Diffraction (XRD)

In X-ray diffraction or scattering (XRD), X-ray photons are utilized to probe the matter. The energy of the emitted radiation is specific for each element. X-rays were

discovered by Roentgen, he called them X-rays because their nature at first was unknown so, X-rays were also called Roentgen rays. The X-rays lie in the range of 0.1 Å < λ < 1000 Å. The penetrating power of X-rays depends on energy.

Principle

X-Ray diffraction effects are observed when electromagnetic radiation impinges on periodic structures with geometrical variations comparable to the length scale of the wavelength of the radiation. X-ray diffraction is based on constructive interference of monochromatic X-rays and a crystalline sample. These X-rays are generated by a cathode ray tube, filtered to produce monochromatic radiation, collimated to concentrate and directed towards the sample [53]. X-rays are generated when high velocity electrons impinge on a metal target. Approximately 1% of the total energy of the electron beam is converted into X-ray radiation. In order to get a narrow beam of X-rays, the X-rays generated by the target material are allowed to pass through a collimator which consists of two sets of closely packed metal plates separated by a small gap. The collimator absorbs all the X-rays except the narrow beam that passes between the gaps [54].

Bragg's Law

Bragg's Law is generally used for investigating the internal structures and crystal structures of different solid compounds. Fig. 3 shows the diffraction of X-ray beam according to Bragg's law [55, 56]. The general relationship between wavelengths of the incident X-rays, angle of incident and spacing between the crystal lattice planes of atoms is known as Bragg's law, as given by Eq. 1.

$$n\lambda = 2d\sin\theta \quad (1)$$

Where d is the spacing between atomic planes in the crystalline phase and λ is the X-ray wave length. The intensity of the diffracted X-rays is measured as a function of the diffraction angle 2θ and the specimen's orientation [55].

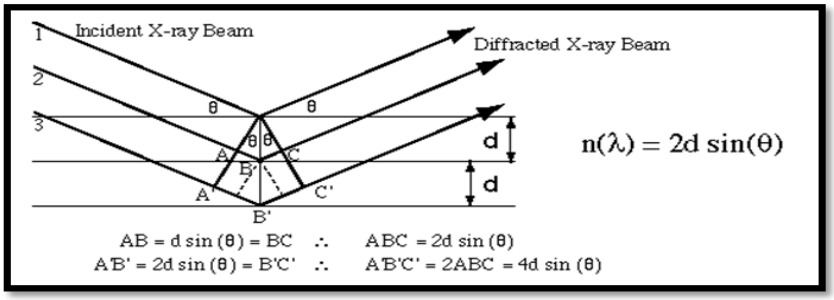

Figure 3 Bragg's Law Reflection

Diffraction peak positions are accurately measured with XRD (fig.4), which makes it the best method for characterizing homogeneous and inhomogeneous strains. Inhomogeneous strains vary from crystallite to crystallite or within a single crystallite and this causes a broadening of the diffraction peaks that increases with the sine of the angle (θ) [56].

Figure 4 XRD apparatus

4.6.2 Energy dispersive X-ray spectroscopy (EDAX)

The fundamental of the EDS technique is by making the use of the X-ray spectrum and emitted by a solid sample bombarded with a focused beam of electrons to obtain a localized chemical analysis. In the periodic table it show all elements starting from atomic number 4 (Be) to 92 (U) can be detected in principle, though not all instruments are equipped for 'light' elements ($Z < 10$). Qualitative analysis consists of the identification of the lines in the spectrum and is fairly straightforward owing to the simplicity of X-ray spectra. During this process, the sample preparation of the electron probe analyses only to a shallow depth, specimens should be well polished so that surface roughness does not affect the results [57].

It’s important to know the atomic structures are according to the Rutherford-Bohr model of the atom is that the electrons orbit around the positive nucleus. In the case of the normal state, the number of orbital electrons equals the number of protons in the nucleus (given by the atomic number, Z). Only certain orbital states with specific energies exist and these are defined by quantum numbers. With increasing Z, orbits are occupied on the basis of minimum energy, those nearest to the nucleus are the most tightly bound, being filled first [57, 58]. This model of the inner structure of the atom is illustrated in fig. 5. The populations of the inner shells are governed by the Pauli Exclusion Principle [58].

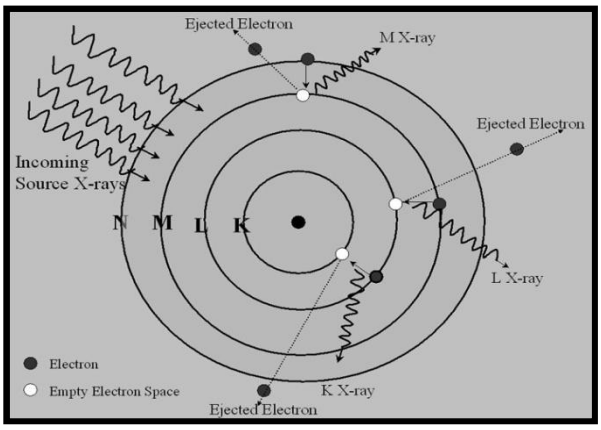

Figure 5 Schematic diagram of inner atomic electron shells

The characteristic X-rays result from electron transitions between inner orbits, which are normally full. An electron must first be removed in order to create a vacancy into which another can fall from an orbit lying farther [58].

4.6.3 Scanning Electron Microscope (SEM)

SEM is a technique that uses electrons as a substitute of light to form an image. Since their development in the early 1950's, SEM has allowed researchers to examine a much bigger variety of specimens. SEM has a large depth of field, which allows more of a specimen to be in focus at one time, SEM also has much higher resolution, so closely spaced specimens can be magnified at much higher levels. Because SEM uses electromagnets rather than lenses, the researcher has much more control in the degree of magnification [59, 60]. It is an instrument that produces a largely magnified image by using electrons instead of light to form an image. A beam of electrons is produced at the top of the microscope by an electron gun and the electron beam follows a vertical path through the microscope, which is held within a vacuum, the beam travels through electromagnetic fields and lenses, which focus the

beam down towards the sample. Once the beam hits the sample, electrons and X-rays are ejected from the sample, as can be observed in fig. 6. The detectors collect these X- rays, backscattered electrons, and secondary electrons and convert them into a signal that is sent to a screen similar to a television screen, which produces the final image . It is generally of non – destructive nature, though sometimes it can cause sample damage due to high energy electron beam irradiation [60].

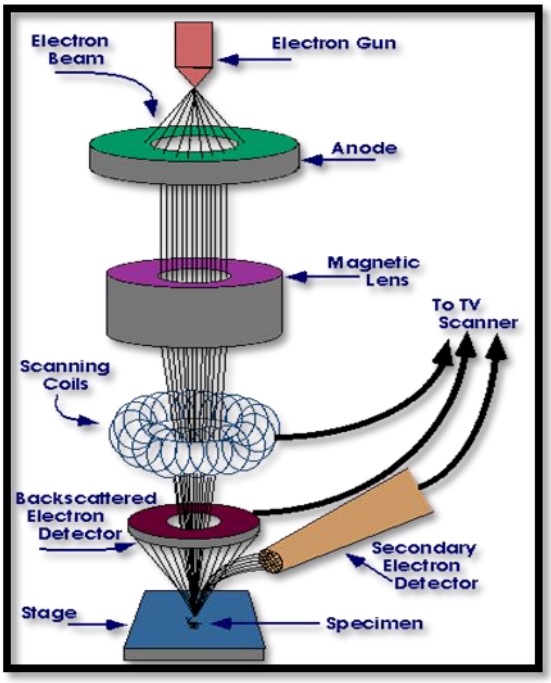

Figure 6 Schematic of SEM

Principle

When an electron beam bombards a solid surface, the incident electrons are scattered. The electron scattering can be divided into two categories, elastic and inelastic scattering, but the speed remains constant. Hence, the kinetic energy of the incident electron remains the same. During an inelastic event, part of the energy of the incident electron is transferred to its colliding partner [60, 61]. Secondary electron, Auger electrons and X-ray are produced by the inelastic scattering events, as shown in fig. 7 [61].

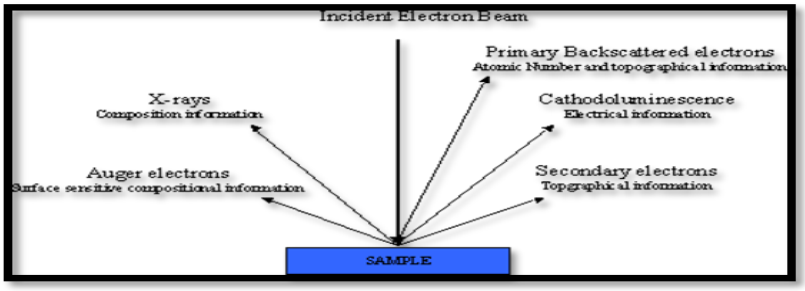

Figure 7 Principle of SEM

Backscattered electrons (BSEs)

A backscattered electron is a scattered primary electron that escapes from the specimen surface before having lost all its energy. A BSE peak lies close to the energy of the incident beam. Primary electrons engaging themselves in small angle scattering travel deeper into the specimen and have a higher probability of suffering from inelastic scattering even if some of them can be backscattered to the specimen surface and escape, these BSEs contribute to the long tail of the energy distribution [61].

Secondary electrons (SEs)

These are defined as electrons emitted from the specimen at less than 50eV. They are predominantly produced by the interactions between energetic electrons and weakly bonded valence electrons of the specimen. The secondary electron peak typically show a most probable energy of 2-5eV [61].

Auger electron

Auger electrons production is an alternative to the characteristic X-ray emission for the relaxation of an atom after the ionization of an inner shell due to a violent electron-electron collision. When an incident electron kicks out an inner shell electron, a vacant electron state is formed. This inner shell vacant state is then filled by another electron from a higher shell, and simultaneously the energy is transferred to another atomic electron that leaves the specimen as an Auger electron. As such the kinetic energy of an Auger electron is the signature of the atom and its chemical environment, and it is independent of the energy of the primary electron (as long as it is high enough to induce inner shell excitation or ionization). Conventionally, Auger electrons escape the specimen with no inelastic energy loss. For most Auger electrons in all common specimens, the inelastic free paths are typically not more than 1nm. Hence, Auger electron spectroscopy and Scanning auger microscopy are surface sensitive techniques [61].

Characteristic X-rays

These are emitted when a hole is created in the inner shell of an atom in the specimen due to inelastic electron scattering, as it can recombine with an outer shell electron. As such, the elemental composition of the specimen can be deduced with energy (Dispersive X-ray spectrometer (EDX)) [61].

Cathode luminescence (CL)

It is the light emission arising from the recombination of electron-hole pairs induced by excitation of electrons in the valence band during inelastic scattering in a semiconducting specimen [61]. Fig. 8 shows the SEM apparatus.

Figure 8 SEM apparatus

4.6.4 Transmission Electron Microscope (TEM)

The Transmission Electron Microscope (TEM) are scientific instruments which use the electrons as light sources to examine objects on a very fine scale. They operate at the same basic principle of the light microscopes; however, as the wavelength of electron is much lower than the light, it is possible to get a resolution thousand times better than a light microscope [62, 63]. A light source at the top of the microscope emits the electrons that travel through vacuum in the column of the microscope. To focus the electrons into a very thin beam, TEM uses electromagnetic lenses. Depending on the density of the material present, some of the electrons are scattered and lost from the beam. At the bottom of the microscope the unscattered electrons hit a fluorescent screen, which gives rise to a 'shadow image' of the specimen with its different parts displayed in varied darkness according to their density [62, 63, 64].

In addition, transmission electron microscope (TEM) forms an image by accelerating the electrons that pass through the specimen. In TEM, electrons are accelerated to 100 KeV or higher (up to 1MeV), projected onto a thin specimen (less than 200 nm) by means of the condenser lens system, and penetrate the sample thickness either undeflected or deflected it can observed in TEM apparatus fig. 10. The greatest advantages that TEM offers

are the high magnification ranging from 50 to 10^6 and its ability to provide both image and diffraction information from a single sample, as shown in fig. 9[64].

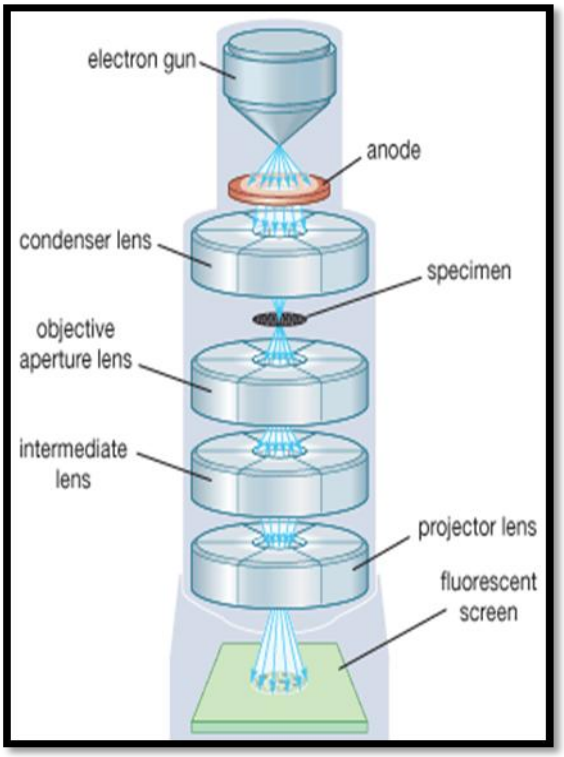

Figure 9 Schematic of TEM

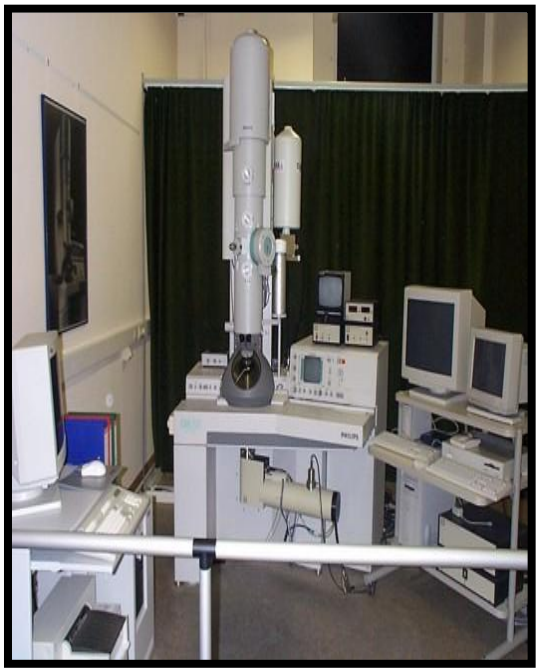

Figure 10 TEM apparatus

4.6.5 Vibrating Sample Magnetometer (VSM)

The principle of vibrating sample magnetometer (VSM) operates on Faraday's Law of Induction, which states that a changing magnetic field will produce an electric field. This electric field can be measured and can tell us information about the changing magnetic field. A VSM is used to measure the magnetic behavior of magnetic materials [65]. If the sample is magnetic, this constant magnetic field will magnetize the sample by aligning the magnetic domains, or the individual magnetic spins, with the field. Stronger the constant field, larger will be the magnetization and magnetic dipole moment of the sample will create a magnetic field around the sample, sometimes called the magnetic stray field. As the sample is moved up and down, this magnetic stray field changes as a function of time and can be sensed by a set of pick-up coils [65, 66, 67].

During this continuous process it can see the alternating magnetic field will cause an electric field in the pick-up coils according to Faraday's Law of Induction [66, 67]. This current will be proportional to the magnetization of the sample, as shown in fig.11.

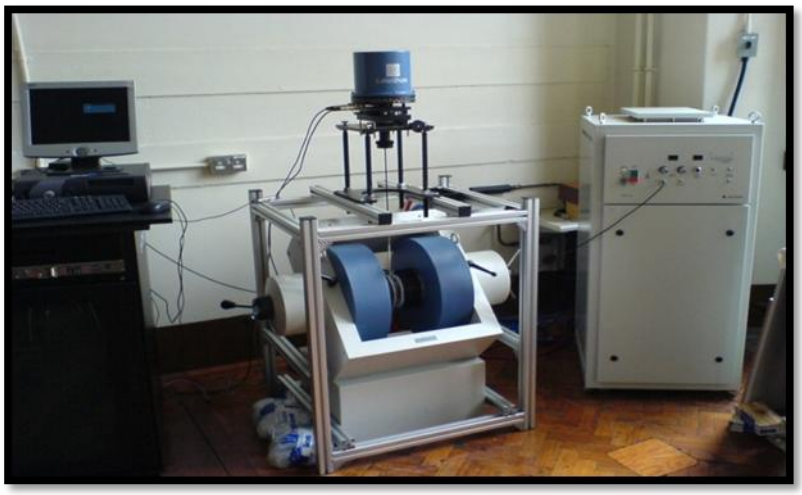

Figure 11 VSM apparatus

A typical measurement of a sample is taken in the following manner:

1. The strength of the constant magnetic field is set.
2. The sample begins to vibrate.
3. The signal received from the probe is translated into a value for the magnetic moment of the sample.

4. The strength of the constant magnetic field changes to a new value. no data is taken during this transition.
5. The strength of the constant magnetic field reaches its new value.
6. The signal from the probe again gets translated into a value for the magnetization of the sample.
7. The constant magnetic field varies over a given range, and a plot of magnetization (M) versus magnetic field strength (H) is generated.

Parts of the VSM

The VSM consists of – Water cooled electromagnet and power supply, Vibration exciter and sample holder, Sensor coils, Hall prop, Amplifier, Control chassis, Lock in amplifier, Meter, Computer interface.

4.6.6 Fourier Transform Infrared Spectrometer (FT-IR)

FT-IR stands for Fourier Transform InfraRed, where some of the infrared radiation is absorbed by the sample and some of it passes through (transmitted) [68]. The resulting spectrum represents the molecular absorption and transmission, creating a molecular fingerprint of the sample [68]. It can identify unknown materials, can determine the quality or consistency of a sample and can determine the amount of components in a mixture [68, 69].

These instruments separate the individual frequencies of energy emitted from the infrared source. An infrared prism works exactly the same as a visible prism which separates visible light into its colors (frequencies). The detector measures the amount of energy at each frequency which has passed through the sample [70]. Fourier transform infrared spectroscopy is preferred over dispersive or filter methods of infrared spectral analysis for the following reasons:

a. It is a non-destructive technique.
b. It can increase speed, collecting a scan every second.
c. It can increase sensitivity – one second scans can be co-added together to ratio out random noise.
d. It has greater optical throughput.
e. It is mechanically simple with only one moving part.

Fourier Transform Infrared (FT-IR) spectrometry was developed in order to overcome the limitations encountered with dispersive instruments. The main difficulty was the slow scanning process. Method for measuring all of the infrared frequencies simultaneously, rather

than individually, was needed. A solution was developed which employed a very simple optical device called an interferometer [70]. Thus, the time element per sample is reduced to a matter of a few seconds rather than several minutes. Most interferometers employ a beam splitter which takes the incoming infrared beam and divides it into two optical beams. One beam reflects off of a flat mirror which is fixed in place. The other beam reflects off of a flat mirror which is on a mechanism which allows this mirror to move a very short distance (typically a few millimeters) away from the beam splitter [70]. The two beams reflect off of their respective mirrors and are recombined when they meet back at the beam splitter, this is because the path that one beam travels is a fixed length and the other is constantly changing as its mirror moves, the signal which exits the interferometer is the result of these two beams "interfering" with each other. The resulting signal is called an interferogram which has the unique property that every data point (a function of the moving mirror position) which makes up the signal has information about every infrared frequency which comes from the source

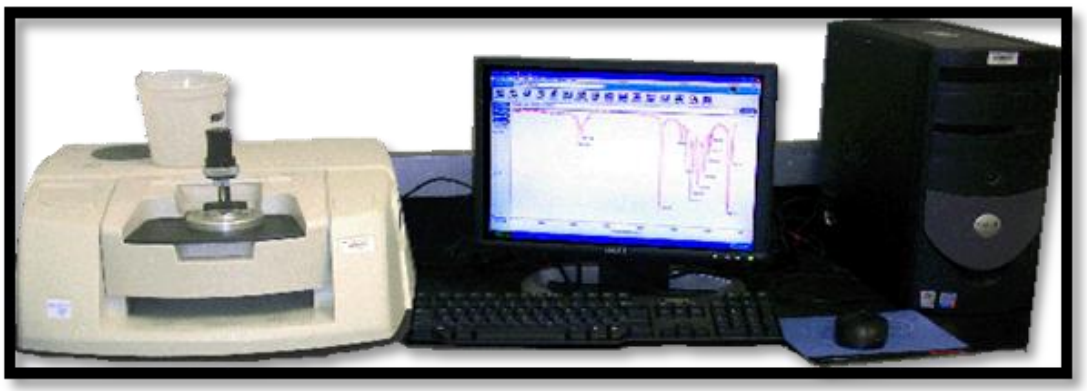

[70]. This transformation is performed by the computer which then presents the user with the desired spectral information for analysis.

Figure12 FT-IR apparatus

5.1 Structural and phase analysis

Fig. 13 (a) shows the XRD diffractogram of potassium ferrite nanoparticles, where all the peaks are indexed and well- matched to the orthorhombic structure with cell parameters a = 5.60Å , b = 11.24Å, c = 15.91Å (File No. 832153). Fig. 13 (b) shows the XRD diffractogram of silica coated potassium ferrite nanoparticles. The crystallite size of synthesized potassium ferrite nanoparticles and silica coated potassium ferrite nanoparticles were calculated by Scherer's formula, as given below:-

$$d = \frac{k\lambda}{\beta \cos \theta}$$

where *k* is the shape factor (*k* = 0.94), λ is the x-ray wavelength, β is the line broadening at half the maximum intensity (FWHM) in radians, and θ is the Bragg angle, *d* is the crystallite size. The crystallite size for potassium ferrite nanoparticles and silica coated potassium ferrite nanoparticles was calculated to be 21 nm and 22.5 nm respectively, indicating that a thin layer of coating has taken place. The XRD patterns are almost similar with difference in the angle (2Θ) range 20-25°.

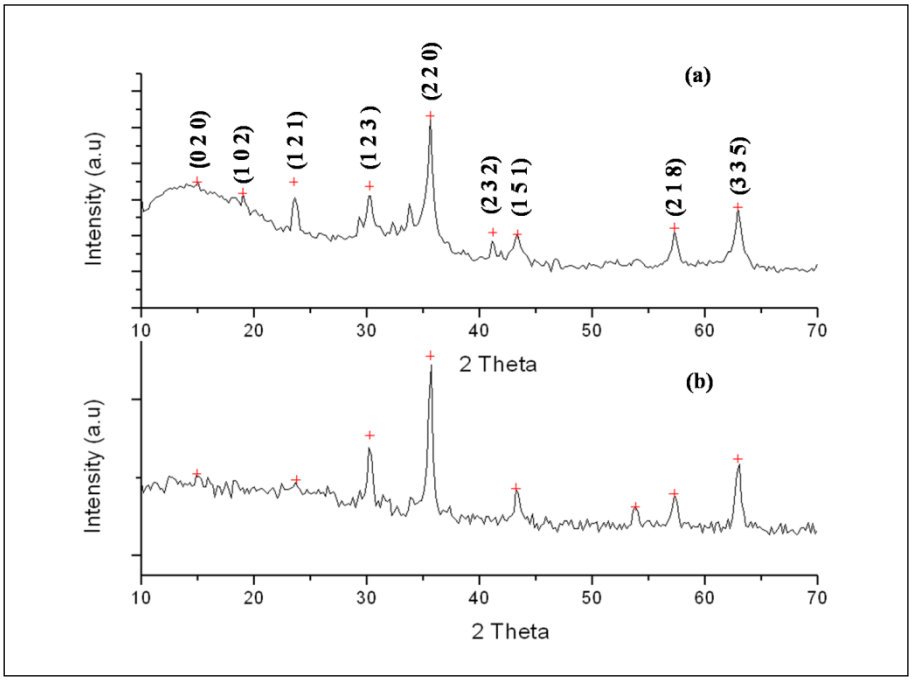

Figure 13 XRD pattern of (a) Potassium ferrite nanoparticles (b) silica coated potassium ferrite nanoparticles

5.2 Morphological Study

5.2.1 SEM and EDAX analysis

SEM micrograph of potassium ferrite nanoparticles, as shown in fig. 14 (a) displays the agglomerated form of the synthesized nanoparticles, similar to the TEM micrograph (fig.16 (a)), owing to their magnetic interactions. The reduced agglomeration in fig. 14 (b) confirms the presence of silica coating on the potassium ferrite nanoparticles and the spherical morphology of the silica coated potassium ferrite nanoparticles can also be well observed.

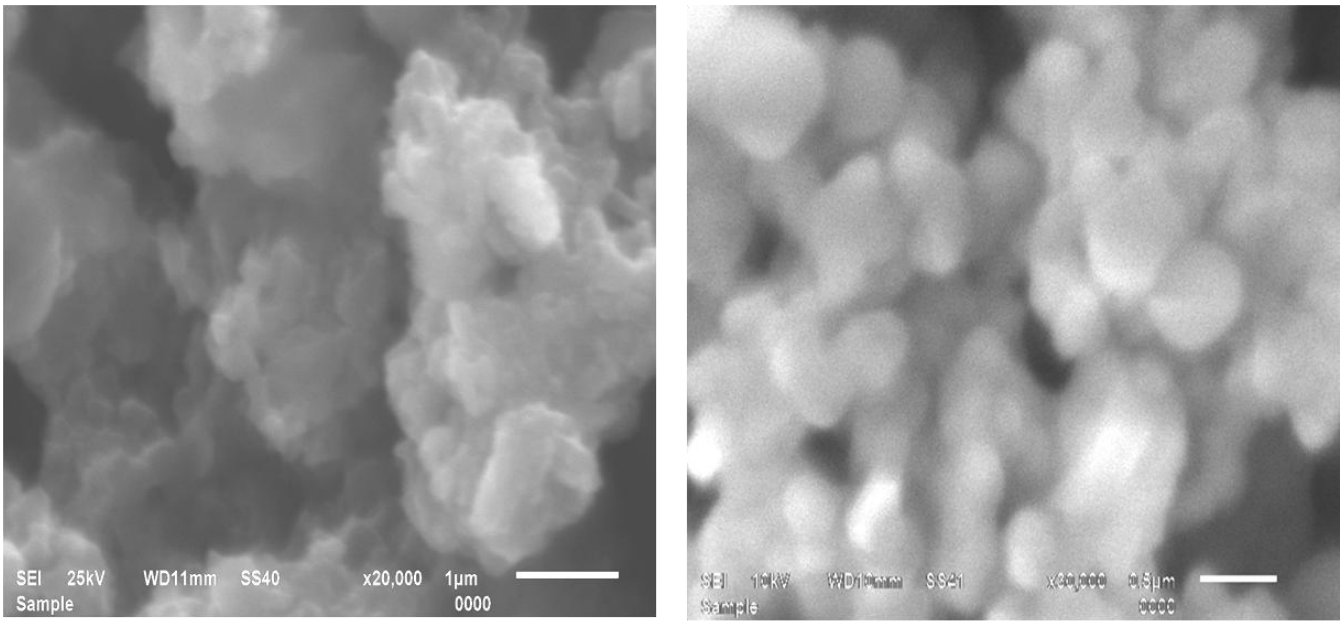

Figure 14 SEM Micrograph of (a) Agglomerated from of synthesized nanoparticles, (b) spherical silica coated potassium ferrite nanoparticles

To further confirm the silica coating on potassium ferrite nanoparticles, EDAX was also performed. Fig. 15(a, b) shows the EDAX spectrum of potassium ferrite nanoparticles and silica coated potassium ferrite nanoparticles respectively. The presence of silica coating on potassium ferrite nanoparticles is well evident.

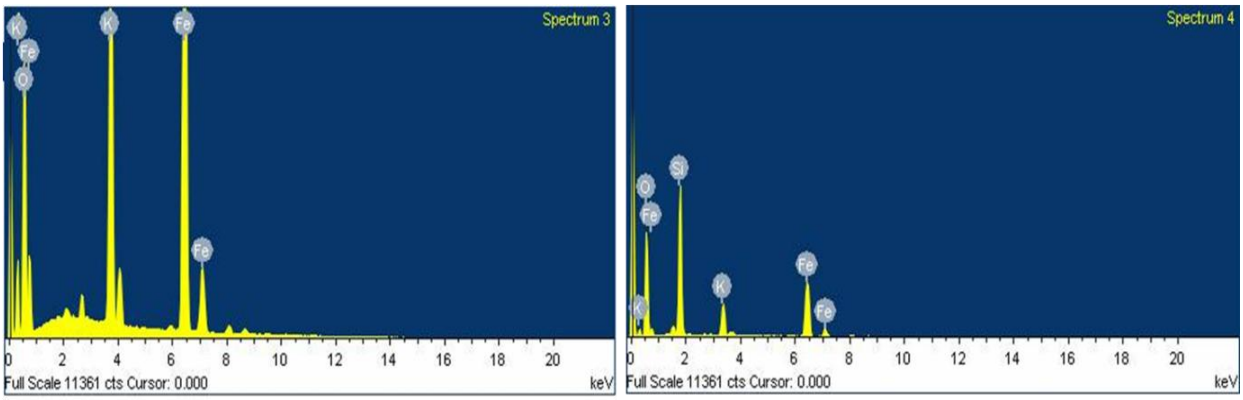

Figure 15 EDAX spectra of (a) potassium ferrite nanoparticles (b) silica coated potassium ferrite nanoparticles

5.2.2 TEM analysis

Fig.16 (a) shows the TEM micrograph of the synthesised potassium ferrite nanoparticles. The agglomeration of the nanoparticles is well observed pertaining to the magnetic interactions between the crystallites. Fig.16 (b) is the TEM micrograph of silica coated potassium ferrite nanoparticles, where the coating of silica on potassium ferrite nanoparticles can be well observed.

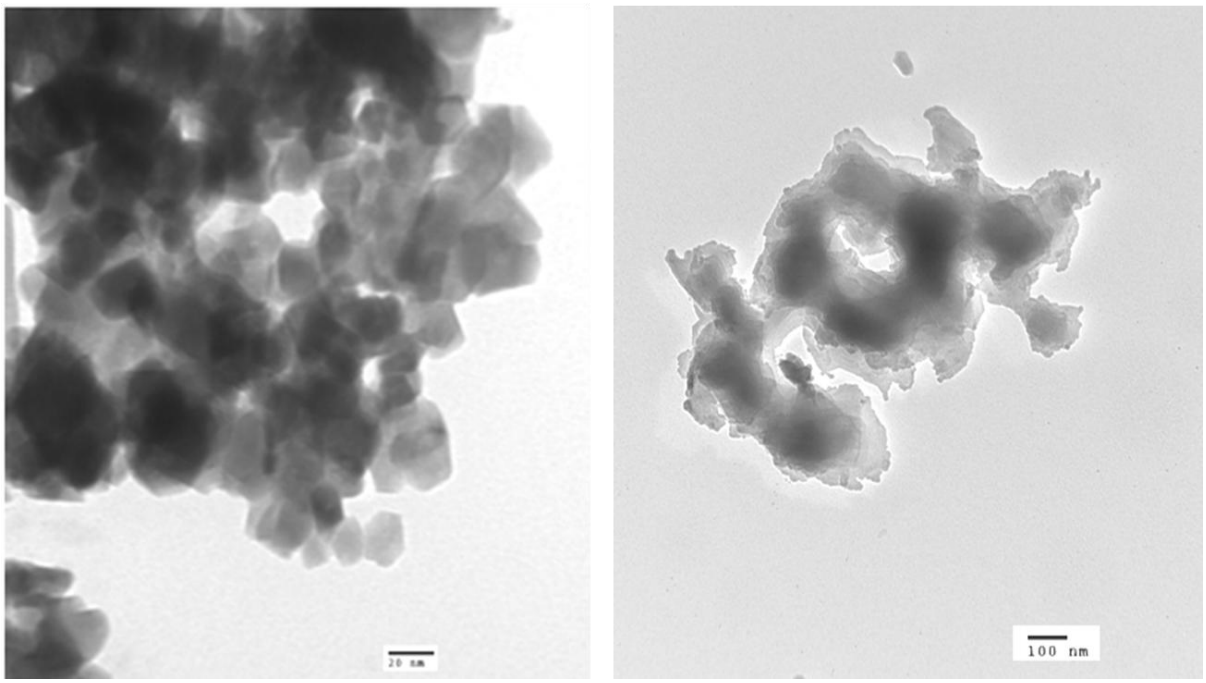

Figure (16) TEM Micrograph of (a) synthesized potassium ferrite nanoparticles, (b) silica coated potassium ferrite nanoparticles

5.3 FTIR Study

FTIR spectra of potassium ferrite nanoparticles and silica coated potassium ferrite nanoparticles is shown in fig.17 (a), (b) respectively. In fig.17 (a), the broad bands at 3156 cm^{-1} and 1633 cm^{-1} are due to stretching and bending vibration of water molecule. The absorption band at 1354 cm^{-1} corresponds to stretching vibration of C-O. The absorption bands at 997 cm^{-1}, 827 cm^{-1} is due to Fe-K system and the one at 687 cm^{-1} is due to Fe-O bond [71].

In fig. 17 (b), water shows an intense characteristic absorption band at 3426 cm^{-1} , assined to O-H stretching. Absorption band at 1632 cm^{-1} is due to scissor bending vibration of molecular water [72]. The peak at 2923 cm^{-1} is due to unreacted TEOS [72]. The absorption band at 1431 cm^{-1} corresponds to stretching vibration of C-O. The characteristic absorption band at 1054 $cm^{-1,}$ in fig. (b) is assigned to the asymmetric stretching vibration of Si-O-Si. The characteristic absorption bands 634 cm^{-1}, 585 cm^{-1} , are attributed to asymmetric stretching of Fe-O-Si [73].

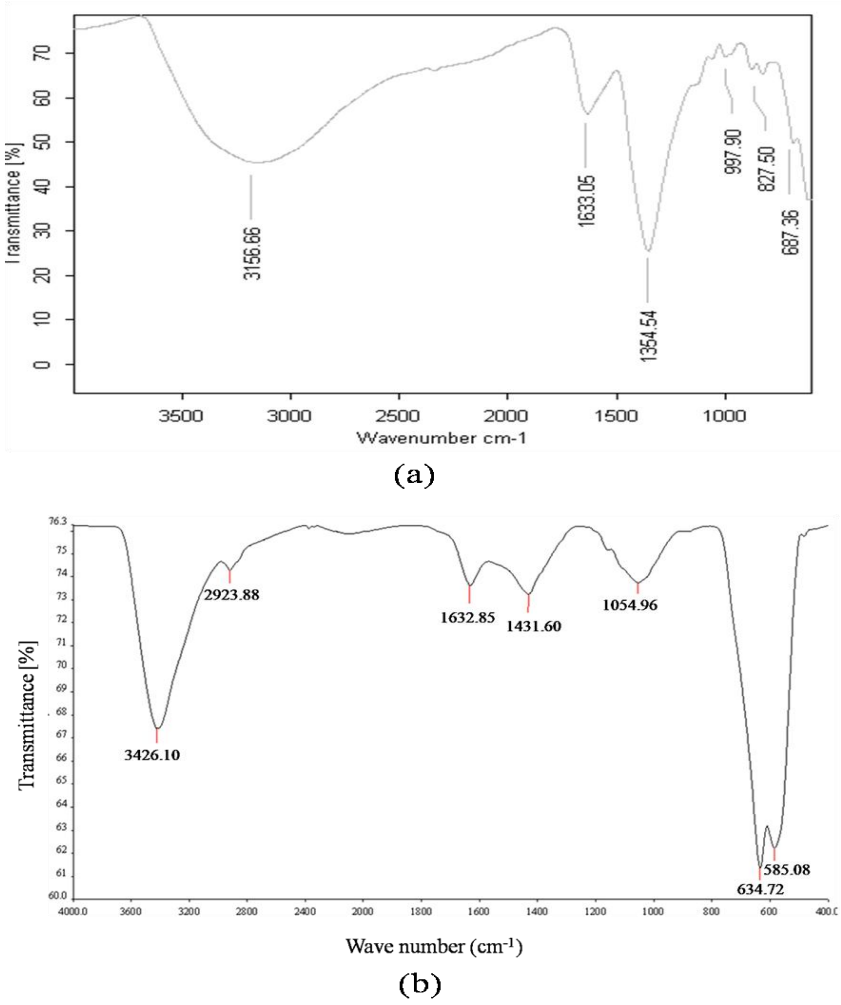

Figure 17 FTIR spectra of (a) potassium ferrite nanoparticle (b) silica coated potassium ferrite nanoparticle

5.4 Magnetic analysis

The magnetic analysis of potassium ferrite nanoparticles and silica coated potassium ferrite nanoparticles was performed on Vibrating sample magnetometer (VSM). In the fig.18, the spectrum (A) corresponds to super paramagnetic behaviour of potassium ferrite nanoparticles and (B) silica coated potassium ferrite nanoparticles. Table 1 gives the respective magnetic values of both the samples, where the reduced magnetization in the case of silica coated potassium ferrite nanoparticles can be attributed to the presence of magnetically dead layer of silica on nanoparticles. The high coercivity in the case of potassium ferrite nanoparticles is because of shape anisotropy, as can be well observed in the TEM micrograph (16) fig. (a)).

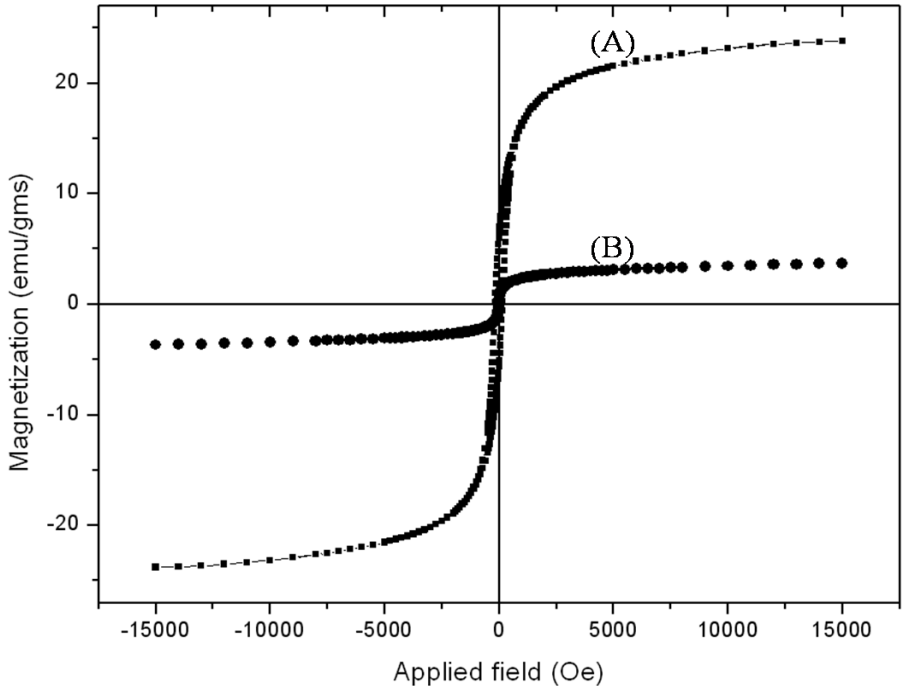

Figure (18) Magnetic spectra of potassium ferrite nanoparticles and silica coated potassium ferrite nanoparticles

Table 1 Magnetic parameters of the synthesized nanoparticles

S.No	Sample	Saturation magnetization (emu/g)	Remanent magnetization (emu/g)	Coercivity (H_c Oe)
1	(A)	23.78	5.79	158.18
2	(B)	3.67	0.24	8.54

Conclusions

The aim of the present research was to synthesize potassium ferrite nanoparticles and to further functionalize/coat it with silica. Following are the conclusions of the work performed:-

- Synthesis of potassium ferrite nanoparticles has been done by sol-gel method and the surface functionalization/ coating with silica has been done by stöber process.

- All the peaks are indexed and well- matched to the orthorhombic structure with cell parameters a = 5.60Å, b = 11.24Å, c = 15.91Å (File No. 832153). The calculated crystallite size for potassium ferrite nanoparticles comes out to be 21 nm and silica coated potassium ferrite nanoparticles comes out to be 22.5 nm. The XRD patterns are almost similar with difference in the angle (2Θ) range 20-25°.

- In the TEM micrograph, the agglomeration of the nanoparticles is well observed pertaining to the magnetic interactions between the crystallites but there is reduced agglomeration in case of silica coated potassium ferrite nanoparticles, as the silica has introduced steric hindrance, resulting in reduced magnetic interactions.

- SEM micrograph of potassium ferrite nanoparticles also displays the agglomerated form of the synthesized nanoparticles, similar to the TEM micrograph and the reduced agglomeration confirms the presence of silica coating on the potassium ferrite nanoparticles, yielding spherical morphology of the silica coated potassium ferrite nanoparticles.

- The presence of silica on potassium ferrite nanoparticles has been further confirmed by EDAX analysis.

- The absorption bands for silica as obtained in the FT-IR study, further confirms the silica coating on potassium ferrite nanoparticles.

- The magnetic analysis of potassium ferrite nanoparticles and silica coated potassium ferrite nanoparticles by Vibrating sample magnetometer (VSM). The reduced magnetization in the case of silica coated potassium ferrite nanoparticles can be attributed to the presence of magnetically dead layer of silica on nanoparticles. The high coercivity in the case of potassium ferrite nanoparticles is because of shape anisotropy.

References

1. RJ. Aitken, Institute of Occupational Medicine Research, 2004
2. E. Roduner, Chemical Society Reviews, 2006,35, 583–592
3. http://c.europa.eu/health/opinions2/en/nanotechnologies/, Health and Consumer Protection Directorate-General-Nanotechnology
4. P. Moriarty, Rep. Prog. Phys.64 (2001) 297–381
5. C. L. Peterson, IEEE Technology and Society Magazine, Wenter 2004
6. N. Ochekpe et al., Tropical Journal of Pharmaceutical Research, June 2009; 8 (3): 265-274
7. M. Arruebo et al., Nano Today 2007, 2, 22-32.
8. A. M. G. C. Dias et al., Biotechnology Advances 29 (2011) 142–155
9. O. M. Koo et al., Nanomedicine: Nanotechnology, Biology and medicine 2005, 1, 193-212.
10. S. C. Mcbain et al., International Journal of Nanomedicine, 2008, 3(2) 169-180.
11. S. Rana, A. Gallo, R. S. Srivastva and R. D. K. Misra, Acta Biomaterialia 2007, 3, 233-242.
12. S. Laurent et al., Chemistry Rev. 2008, 108, 2064-2110.
13. C. S. KurodaI et al., IEEE Transactions on Magnetic, Vol.42, No. 10, October 2006.
14. J. Gwang Lee et al., Journal of Magnetism 177-181 (1998) 900-902.
15. K. Maaz et al., Journal of Magnetism and Magnetic Materials 321 (2009) 1838-1842.
16. I. Elahi et al., African Journal of Pure and Applied Chemistry Vol. 6(1), pp. 1-5, 2012.
17. A. Pradeep et al., Journal of Magnetism and Magnetic Materilas 320 (2008) 2774-2779
18. M. Atif et al., Solid State Communications 138 (2006) 416–421
19. M. Meng Lin et al., 2010.
20. J. Kim et al., Chemistry Soc. Rev., 2009, 38, 372–390.
21. S. K. Sahoo et al., Vol. 8, No. 24 December 2003.
22. N. A. Ochekpe et al., Tropical Journal of Pharmaceutical Research, 2009; 8 (3): 275-287.
23. M. Liong et al., 2008, 2(5), 899-896
24. S. Li et al., New Journal Chemistry, 2009, 33, 2414–2418.
25. P. C. Wu et al., Chemistry Eur. J. 2007, 13, 3878 – 3885.
26. N. S. Kommareddi et al., Chemistry Materials 1996, 8, 801-809.
27. N. A. D Burke et al., Chemistry Materials 2002, 14, 4752-4761.

28. Q. Chen et al., 2008, 24, 650-653.
29. Chen et al., Journal of Nanotechnology in Engineering and Medicine 1 (2010) 011009-1.
30. K. E. Scarberry et al., PhD Thesis, School of Chemistry and Biochemistry, Georgia Institute of Technology, 2009.
31. S. Rana et al., Materials Chemistry and Physics 2010, 124, 264-269.
32. Z. Zi et al., Journal of Magnetism and Magnetic Materials 2009, 321, 1251–1255.
33. K. Maaz et al., Journal of Magnetism and Magnetic Materials 2007, 308, 289–295.
34. S. O. Gyergyek et al., Nanopart Res 2010, 12, 1263–1273.
35. B. G. Toksha et al., Solid State Communications 2008, 147, 479–483.
36. J. Jiang et al., Current Applied Physics 2010, 10, 284–288.
37. M. L. Esteves et al., Journal of Magnetism and Magnetic Materials 2009, 321, 3061-3066.
38. H. Yang et al., Biomaterials 2010, 31, 3667-3673.
39. H. Yin et al., Biomaterials 2005, 26, 5818-5826.
40. W. Voit et al., Vol. 676 2001 Materials Research Society.
41. Xu et al., Journal of Magnetism and Magnetic Materials 309 (2007) 307–311.
42. M. H. Amtenbrink et al., Nanostructured Materials for Biomedical Applications, 2009.
43. N. Trana et al., Journal of Materials Chemistry, 2010.
44. A. L. Andrade et al., Cerâmica 55 (2009) 420-424
45. A. Tomitaka et al., Journal of Magnetism and Magnetic Materials 2009, 321, 1482-1484.
46. http://www.nanotech-now.com/, Nanotechnology Now
47. P. Saravanan et al., Nanomaterials, Journal, 58, No. 4, July 2008, pp. 504-516
48. http://www.news-medical.net, Medical Science News
49. https://www.llnl.gov/str/May05/Satcher.htm, Science and Technology
50. I. A.M. Ibrahim et al., Journal of American Science, 2010;6(11).
51. K. Sreenivasa Rao et al., Journal of Colloid and Interface Science289 (2005) 125–131.
52. D. Adolfo Santamarı´a Razoet al., J Nanopart Res (2008) 10:1225–1229.
53. B.K Tanner et al., Applied surface science 182 (2001) 202-208.
54. http://gitam.edu/eresource/nano/
55. L. B. Ugemann et al., Nuclear Instruments and Methods in Physics Research A 531 (2004) 292–301.
56. L. P´erez et al., Revista maxicanade F Icanade, 50(2)96–98, April 2004
56. http://micron.ucr.edu/public/manuals/EDS-intro.pdf
57. http://www.the-iom.org/assets/files/SEM-TEM.pdf
58. http://micron.ucr.edu/public/manuals/EDS-intro.pdf

59. http://www.the-iom.org/assets/files/SEM-TEM.pdf
60. C. T. K. H. Stadtländer et al., Modern Research and Educational Topics in Microscopy, 2007
61. L.S. Chumbley et al., JOM, 47 (9) (1995), pp. 13-17.
62. W. C. Nixon, Application in Biology. (May 27, 1971), pp. 45-50.
63. Brigitte B. et al., 2005
64. G. Wu et al., Ultramicroscopy109 (2009) 137–1325e matching
65. http://uweb.txstate.edu/~ab35/manuals/VSM/vsm.pdf
66. http://uweb.txstate.edu/~ab35/manuals/VSM/vsm.pdf
67. P. Stamenova et al., Journal of applied physics 99, 08D912(2006).
68. G. E. A. Swann et al., Clim. Past, 7, 65–74, 2011
69. Z. Movasaghi et al., Applied Spectroscopy Reviews, 43: 134–179, 2008.
70. C.C. Homes, Condensed Matter Physics & Materials Science Department Brookhaven National Laboratory, 2011.
71. S. rana et al., Materials Chemistry and Physics 124 (2010) 264-269.
72. A. Beganskiene et al., Materials Science, Vol. 10, No. 4. 2004, 287-280.
73. N. Andhariya et al., J Nanopart Res (2011) 13:3619-3631.